Reaction Coordinate Analysis of the S_2-S_1 Internal Conversion of Phenylacetylene

Yoshiaki Amatatsu*

Faculty of Engineering and Resource Science, Akita University, Tegata Gakuen-cho, Akita 010-8502, Japan

Received: July 20, 2005; In Final Form: February 1, 2006

The reaction coordinate of the S_2-S_1 internal conversion (IC) of phenylacetylene (PA) was analyzed using the ab initio complete active space self-consistent field (CASSCF) method. In the first process after electronic excitation into S_2, the aromatic benzene ring is transformed into a nonaromatic quinoid structure. The ethynyl part (−C≡CH) takes an incomplete allenoid structure in which the CC bond elongates to an intermediate value between typical C≡C triple and C═C double bonds, but the bend angle of −CCH is 180°. In the second process, PA takes a complete allenoid structure with an out-of-plane location of the β-H atom (i.e., the H atom of the ethynyl part) and a further elongation of the CC bond so that PA is most stable in S_2 (S_2-bent). The conical intersection between S_2 and S_1 (S_2/S_1-CIX) is located near the S_2-bent geometry and is slightly unstable energetically. After transition at S_2/S_1-CIX, PA quickly loses both quinoid and allenoid structures and recovers the aromaticity of the benzene ring in S_1. Analysis of the dipole moment along the reaction coordinate shows that the weak electron-withdrawing group of the ethynyl part in S_0 suddenly changes into an electron-donating group in S_2 after the main transition of S_0-S_2. The photoinduced change of the dipole moment is a driving force to the formation of a quinoid structure in S_2. Regarding the benefit of the reaction coordinate analysis of the multidimensional potential energy surfaces of PA, the present picture of the IC process is much more elaborate than our previous representation (Amatatsu, Y.; Hasebe, Y. *J. Phys. Chem. A* 2003 *107,* 11169−11173). Vibrational analyses along the reaction coordinate were also performed to support a time-resolved spectroscopic experiment on the S_2-S_1 IC process of PA.

1. Introduction

Internal conversion (IC) from a highly excited state to the lowest state (i.e., S_n-S_1, $n \geq 2$) is recognized as an important process in the photochemistry of π-conjugated molecules.[1] Regarding the benefit of the recently developed femtosecond time-resolved spectroscopic technique, it has been confirmed in various π-conjugated molecules that the S_n-S_1 IC process is extremely rapid: it requires not more than approximately a few hundred femtoseconds.[2−7] However, the extreme rapidity of the IC process prevents us from obtaining more detailed spectroscopic information with a reliable signal/noise ratio. Particularly, an important conformation of the conical intersection (CIX) within which radiationless transition takes place[8] is difficult to determine experimentally because the CIX is only a passing point. Therefore, the mechanism of the IC process remains far from realization. To compensate for the disadvantages of experiments, a determination of CIX using a reliable ab initio calculation is a useful alternative approach. However, a CIX is much more difficult to locate than a stable geometry or saddle point of a specific state because a CIX is a cusp at which two potential energy surfaces cross. Recently, we determined CIXs of several important π-conjugated polyatomic organic molecules using an ab initio complete active space self-consistent field (CASSCF) method.[9−11] All CIXs that we determined have a common feature: some (more than two) internal coordinates deviate significantly from those at the equilibrium geometry in S_0. It remains unclear whether the deviations of internal coordinates occur simultaneously or stepwise to reach the S_2/S_1-CIX. Calculation of intrinsic reaction coordinates seems to be a good approach to resolve that question because the geometrical changes that depend on the reaction coordinate indicate which of the modes among the internal coordinates couple with each other on multidimensional potential energy surfaces. In other words, the pursuit of the reaction coordinate can lend some insight into the internal vibrational redistribution in the IC process. In this study, we applied reaction coordinate analysis to the S_2-S_1 IC process of phenylacetylene (PA). Therefore, we propose a more elaborate model than our previous one[9] and thereby promote a sophisticated time-resolved spectroscopic experiment.

Herein, we summarize the experimental findings related to the S_2-S_1 IC of PA. We review the photochemistry of PA in our previous report. (i) The S_0-S_2 absorption band is strong with diffuse peaks, whereas the S_0-S_1 peak is weak with a rotationally resolved structure.[12,13] (ii) The diffuse peaks that are overlapped in the S_0-S_2 broad absorption band have a constant interval of 1846 ± 15 cm^{-1}.[14] (iii) The S_2-S_1 IC is very fast (relaxation time constant = 54 fs), whereas the S_1-S_0 IC is much slower (9.4 and 63 ps)[3].

2. Method of Calculations

For the present calculations, we adopted a larger scale of 10 electrons in 10 orbitals CASSCF [denoted as (10,10)CASSCF], of which five π-occupied and the lowest five π*-unoccupied orbitals are included. This same basis set was used in previous calculations [i.e., the Huzinaga−Dunning double-ζ (DZ) basis set augmented by polarization ($\alpha_d = 0.75$) on carbon atoms].[9] However, we newly optimized several important conformations using a state-specific (10,10)CASSCF to check the extent to which the size of the active space affects geometries. Next, we calculated the reaction path on the S_2 surface starting from the equilibrium geometry in S_0 (S_0 geometry). This reaction path

* E-mail: amatatsu@ipc.akita-u.ac.jp. Fax: +81-18-889-2601.

10.1021/jp054008c CCC: $33.50 © 2006 American Chemical Society
Published on Web 03/16/2006

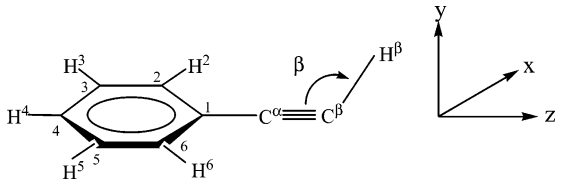

Figure 1. Numbering of atoms and definition of coordinates in phenylacetylene.

(denoted as path A) finally converges at the most stable geometry in S_2 (S_2-bent). Then, we followed two types of reaction paths starting from S_2/S_1-CIX. One converges into the S_2-bent geometry in S_2 (path B); the other converges into the globally stable geometry in S_1 (S_1 geometry) (path C). We also followed several reaction paths from the $C^{\beta}H^{\beta}$ out-of-plane (OP) bent geometries (see Figure 1) to examine the effect of the initial bending motion on the dynamics. In all present ab initio calculations, we used the GAMESS program.[15]

3. Results and Discussion

3.1. Geometries at Important Conformations. We first make a brief mention of the geometries at important conformations for later discussion on the IC process, but we discussed them in detail in relation to each electronic structure in our previous work.[9] As listed in Table 1, the present (10,10)CASSCF geometries are not much different from our previous (10,9)CASSCF ones.[9] Regarding the S_0 geometry, the aromatic benzene ring has some resonance with the ethynyl (C≡CH) part, so that the linkage C^1C^{α} bond shrinks slightly. The S_1 geometry is characterized by an enlarged benzene ring because the CC bonds of the benzene ring weaken in S_1 as a result of a locally $\pi-\pi^*$ excited state within the benzene ring. The linkage C^1C^{α} bond is shorter than that at theS_0 geometry, which implies that the resonance between the benzene ring and the ethynyl part becomes stronger in S_1. The stable geometry in S_2 under constraint of C_{2v} symmetry (S_2-planar) loses the aromaticity of the benzene ring and comes to adopt a quinoid structure, i.e., C^1C^2, C^3C^4, C^4C^5, and C^1C^6 become longer, whereas C^2C^3 and C^5C^6 become shorter. As for the ethynyl part, the $C^{\alpha}C^{\beta}$ bond elongates to take an intermediate value between triple C≡C and double C═C bonds; the linkage C^1C^{α} bond resembles a normal C═C double bond. However, it is hard to say that the $C^1C^{\alpha}C^{\beta}$ part is an allenoid skeleton in which both CC bonds are similar to normal double bonds. Therefore, we infer that the S_2-planar geometry is an incomplete allenoid structure. At the globally stable S_2-bent geometry, PA adopts a complete allenoid structure in which the $C^{\alpha}C^{\beta}$ bond becomes longer and comes to resemble a normal C═C double bond; the $-C^{\alpha}C^{\beta}H^{\beta}$ bend angle β is approximately 120°. The $C^{\beta}H^{\beta}$ bond distance at the S_2-bent geometry differs from that at the S_2-planar geometry. The former is a typical C−H bonded to a C═C double bond (i.e., ═C−H), whereas the latter is a typical C−H bonded to a C≡C triple bond (i.e., ≡C−H). The difference between these $C^{\beta}H^{\beta}$ bonds can be interpreted in relation to their respective electronic structures. For the S_2-bent geometry, respective hybridizations of the C^1, C^{α}, and C^{β} atoms are sp^2, sp, and sp^2, whereas they are sp^2, sp, and sp at S_0 geometry and S_1 geometry. Therefore, the H^{β} atom at the S_2-bent geometry favors a location out of the plane of the remaining part. In addition, S_2/S_1-CIX takes a structure similar to the S_2-bent geometry. This implies that a crossing point of S_2/S_1-CIX is located in the vicinity of the S_2-bent geometry. We did not newly optimize an S_2/S_1-CIX configuration using the present method of (10,10)CASSCF because of the heavy computational demands in the location of S_2/S_1-CIX; instead, we used the geometrical parameters yielded by our previous (8,8)CASSCF method. We verified the energy difference between S_2 and S_1 at S_2/S_1-CIX using (10,10)CASSCF and MRMP2. Thereby, we found that the energy differences are too small (0.015 eV by CASSCF, 0.099 eV by MRMP2) to be a CIX. These small differences imply that S_2/S_1-CIXs by a larger scale of (10,10)CASSCF or MRMP2 are not very different from that by (8,8)CASSCF.

3.2. Reaction Path from S_0 Geometry into S_1 Geometry. In this subsection, we describe the main interest of the reaction path from the S_0 geometry into the S_1 geometry. In Figure 2, we show the energy profiles of paths A−C. Path A, for which the reaction coordinate is labeled s_A, starts from the S_0 geometry in S_2 and converges into the most stable geometry in S_2 (i.e., S_2-bent) (see Figure 2a). Paths B and C, for which the reaction coordinate is labeled as s_{BC} in Figure 2b, start from S_2/S_1-CIX and converge into the S_2-bent geometry in S_2 and the S_1 geometry in S_1, respectively. Figure 3 shows characteristic geometrical parameters along the reaction coordinate. From energy profiles and geometrical changes, we can determine that the S_2-S_1 IC process of PA consists of four subprocesses, denoted as PR1, PR2, PR3, and PR4 hereafter. In the following paragraphs, we discuss these processes in relation to geometrical changes.

In PR1 ($0 \le s_A \le 0.895$ in Figure 2a), the energy in S_2 is lowered quickly from the S_0 geometry. The skeletal bond distances change greatly (see Figure 3a). The $C^{\alpha}C^{\beta}$ bond elongates to an intermediate value between a typical C≡C triple bond and a C═C double bond. The linkage C^1C^{α} bond shrinks into a normal double bond in coincidence with elongation of

TABLE 1: Characteristic Optimized Parameters of PA by (10,10)CASSCF

	S_0	S_1	S_2-planar	S_2-bent	S_2/S_1-CIX[a]
			Bond Distances (Å)		
$R(C^{\alpha}-C^{\beta})$	1.215 (1.216)[b]	1.221 (1.210)	1.289 (1.281)	1.331	1.338
$R(C^1-C^{\alpha})$	1.448 (1.448)	1.424 (1.417)	1.360 (1.358)	1.359	1.358
$R(C^1-C^2)$	1.405 (1.395)	1.447 (1.446)	1.475 (1.456)	1.477	1.482
$R(C^2-C^3)$	1.398 (1.395)	1.438 (1.438)	1.368 (1.372)	1.364	1.370
$R(C^3-C^4)$	1.401 (1.398)	1.432 (1.432)	1.470 (1.445)	1.454	1.411
$R(C^4-C^5)$	1.401 (1.398)	1.432 (1.432)	1.470 (1.445)	1.454	1.411
$R(C^5-C^6)$	1.398 (1.395)	1.438 (1.438)	1.368 (1.372)	1.364	1.370
$R(C^{\beta}-H^{\beta})$	1.058 (1.059)	1.058 (1.059)	1.057 (1.058)	1.078	1.080
			Bond Angles (deg)		
$\alpha(-C^1C^{\alpha}C^{\beta})$	180.0 (180.0)	180.0 (180.0)	180.0 (180.0)	177.3	179.7
$\beta(-C^{\alpha}C^{\beta}H^{\beta})$	180.0 (180.0)	180.0 (180.0)	180.0 (180.0)	125.6	121.3
			Dihedral Angles (deg)		
$-C^1C^{\alpha}C^{\beta}H^{\beta}$	–	–	–	180.0	180.0

[a] Values are taken from ref 9. [b] Values in the parentheses taken from ref 9 were obtained by (10,9)CASSCF.

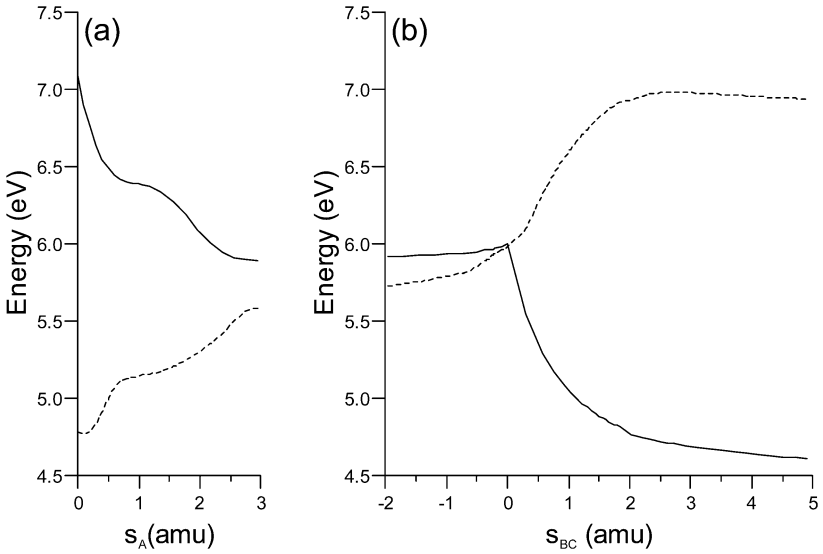

Figure 2. Potential energy profiles (solid line) along the reaction coordinate by means of (10,10)CASSCF. The dotted line represents the potential energy of the counter state. (a) Path A. (b) Paths B and C.

$C^{\alpha}C^{\beta}$. As for the bond distances in the benzene ring, C^1C^2 (and C^1C^6) and C^3C^4 (and C^4C^5) become longer in coincidence with elongation of $C^{\alpha}C^{\beta}$, whereas C^2C^3 (and C^5C^6) shrink into a normal C═C double bond. In other words, the aromaticity of the benzene ring is lost, and a quinoid structure is formed. As shown in Figure 3b, the $C^{\beta}H^{\beta}$ bond distance remains almost unchanged from that of a typical ≡C−H bond. The bend angle β is almost constant at 180°, meaning that the hybridizations of both the C^{β} and C^{α} atoms are sp, even at the end of PR1. Therefore, PR1 is interpreted as the formation of a quinoid structure, almost retaining a C_{2v} planar geometry. The end of PR1 corresponds to an incomplete allenoid of S_2-planar geometry mentioned above.

In the second process of PR2 ($s_A \geq 0.895$), where PA reaches the most stable S_2-bent geometry, the following characteristic changes occur: The $C^{\alpha}C^{\beta}$ bond elongates into a normal C═C double bond, whereas C^1C^{α} remains almost unchanged as a normal C═C double bond. The $C^{\beta}H^{\beta}$ distance changes from a typical ≡C−H bond into ═C−H bond in coincidence with elongation of $C^{\alpha}C^{\beta}$. The bend angle β also changes from 180° to ca. 120°. These changes in geometry reflect the change in the hybridization of the C^{β} atom from sp into sp^2 in PR2. Therefore, PR2 is interpreted as a completion process of an allenoid structure of the ethynyl part.

During the passage from the S_2-bent geometry to S_2/S_1-CIX [i.e., PR3 ($s_{BC} \leq 0.0$)], the energy profile is inclined slightly by 0.104 eV. All geometrical parameters change only slightly (see Figure 3c,d). These facts imply that electronically excited PA in S_2 that starts from the S_0 geometry is unlikely to be trapped at the most stable of S_2-bent geometry. It immediately passes over S_2/S_1-CIX to relax into S_1.

After relaxation into S_1 at S_2/S_1-CIX [i.e., PR4 ($s_{BC} \geq 0.0$)], the energy decreases monotonically into the most stable geometry in S_1 (i.e., S_1 geometry) after the transition at S_2/S_1-CIX (see Figure 2b). The characteristic allenoid and quinoid structures disappear quickly. That is, $C^{\alpha}C^{\beta}$ shrinks into a normal triple C≡C bond, and C^1C^{α} elongates from a normal C═C double bond. The benzene ring recovers its aromaticity so that PA in S_1 relaxes into an S_1 geometry characterized by an enlarged benzene ring. Coincident with these changes, the $C^{\alpha}C^{\beta}H^{\beta}$ part again takes a linear shape (i.e., $\beta = 180°$), and the $C^{\beta}H^{\beta}$ bond shrinks into a typical ≡C−H bond. These geometric changes after the transition into S_1 at S_2/S_1-CIX can be understood in relation to the change of hybridization of the C^{β} atom from sp^2 into sp.

On the basis of the above discussion, we can depict the S_2-S_1 IC of PA; it is shown schematically in Figure 4. We also include a comment on the definitions of three coordinates in Appendix 1. In the first process, immediately after electronic excitation into S_2 at the S_0 geometry, the PA skeleton changes greatly, maintaining a substantially planar structure. That is, the aromatic benzene ring changes to adopt a quinoid structure, and the ethynyl part changes into an incomplete allenoid structure. In the second process, PA comes to take a complete allenoid structure in which two bonds of C^1C^{α} and $C^{\alpha}C^{\beta}$ are similar to normal double bonds and the H^{β} atom is located out of the plane of the other part. In the third process, PA reaches S_2/S_1-CIX with a slightly inclined energy profile against the most stable geometry in S_2 (S_2-bent). In the fourth process, PA relaxes into S_1 at S_2/S_1-CIX and quickly recovers its aromaticity with an enlarged benzene ring. The ethynyl part changes from an allenoid ═C═CH structure into −C≡CH. Finally, PA relaxes into the stable S_1 geometry, which is characterized as an enlarged benzene ring with C_{2v} geometry. In the series of processes mentioned above, the important internal coordinates are different. In other words, the geometrical changes of some internal coordinates in one process bring about those of other internal coordinates in the following process. Therefore, we conclude that the strong mode couplings of the potential energy surfaces, which depend on the reaction coordinate, are a driving force for the effective and fast S_2-S_1 IC process of PA, despite the fact that the S_2/S_1-CIX is far from S_0 geometry.

In concluding this subsection, we note that more sophisticated MRMP2 reaction coordinate analyses will change the present scheme of (10,10)CASSCF. Figure 5 depicts the energy profile by MRMP2 energetic correction against that by CASSCF shown in Figure 2. The features of the energy profile are retained even by MRMP2 energetic correction, except that the energies are reduced by ca. 1 eV. Consequently, we infer that our present model will not be changed greatly, even by a more sophisticated MRMP2 reaction coordinate analysis.

3.3. Effect of the Initial Bending Motion around the S_0 Geometry. The electronically excited PA in S_2 is likely to move around the reaction path described in the preceding subsection, even taking into account the zero-point vibrations in S_0 around the S_0 geometry. However, to characterize the process more

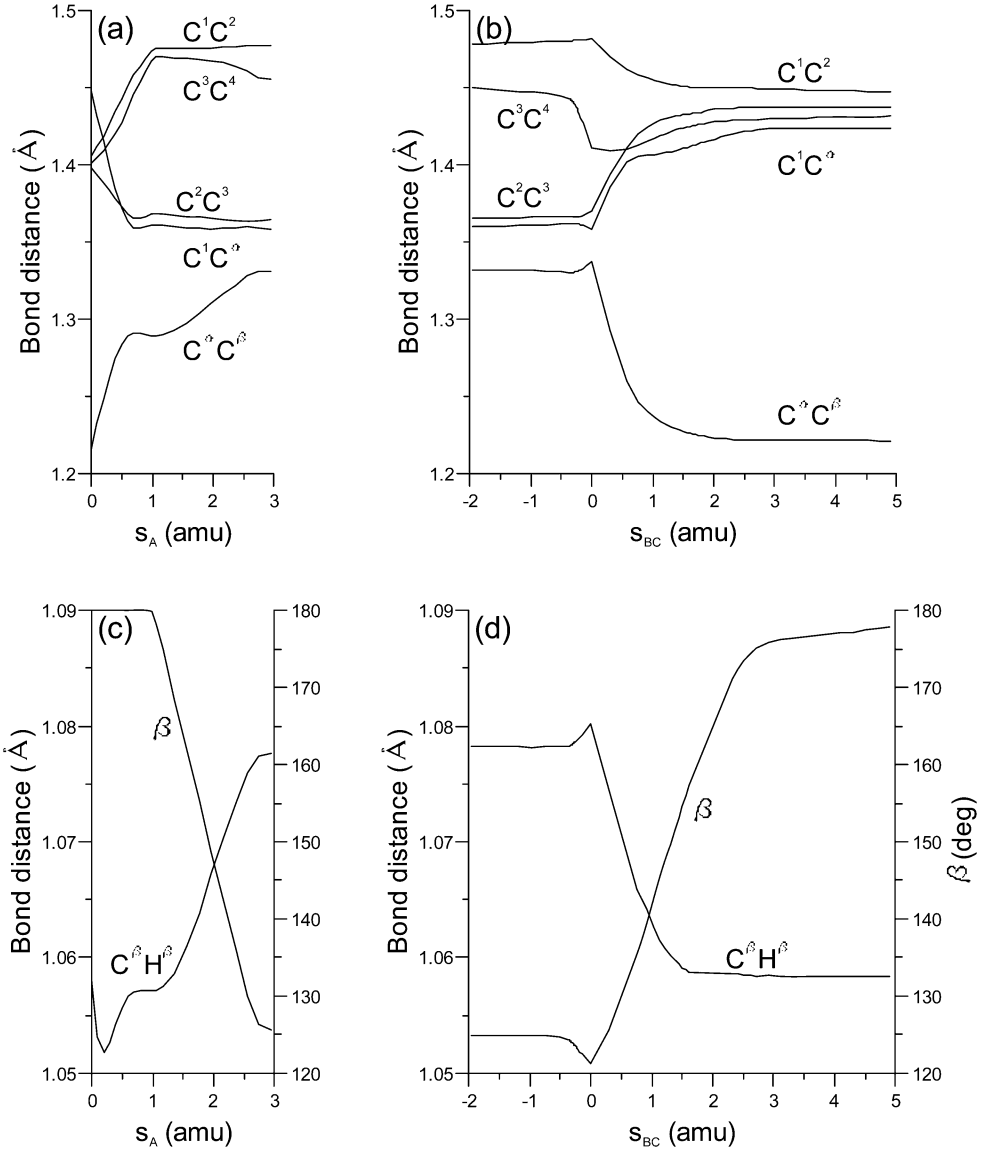

Figure 3. Characteristic geometrical parameters along the reaction coordinate for (a,b) path A and (c,d) paths B and C. a and c describe changes of bond distances of the PA skeleton. The bond distances of C^1C^6, C^5C^6, and $C^4C,^5$ which are not drawn, are substantially identical to those of C^1C^2, C^2C^3, and C^3C^4, respectively. b and d describe those of the $C^\beta H^\beta$ bond distance and the $-C(C^\beta H^\beta$ bending angle β.

realistically, it is worthwhile commenting on the degree to which zero-point vibrations in S_0 affect the IC process after electronic excitation into S_2. For the following two reasons, we specifically address the effect of the initial $C^\beta H^\beta$ OP bending motion that is exerted: (i) the $C^\beta H^\beta$ OP bending vibration is of a low-frequency mode and (ii) a large geometrical change from S_0 geometry into S_2/S_1-CIX is the bend angle of $-C^\alpha C^\beta H^\beta$.

Figure 1 shows that the direction of the OP motion corresponds to the y coordinate. For that reason, the H^β atom was placed out of the plane of the remaining part by $y = 0.05$ ($\beta = 177.3°$), 0.10 ($\beta = 174.6°$), 0.15 ($\beta = 171.9°$), and 0.21 Å (more accurately, $y = 0.2113$, $\beta = 168.5°$), keeping the $C^\beta H^\beta$ distance at that of the S_0 geometry. We hereafter call these configurations S_0B05, S_0B10, S_0B15, and S_0B21, respectively. Appendix 2 describes the determination of the OP distance of S_0B21 (i.e., $y = 0.21$ Å), which is approximately the amplitude of the $C^\beta H^\beta$ OP bending motion. Figure 6 depicts energy profiles of the bent geometries and the S_0 geometry. The energy profiles of the bent geometries apparently differ from that of the S_0 geometry. More careful inspection, however, reveals a common feature: each energy profile has an inflection point. Table 2 reports information related to those inflection points. This table reveals that the bend angle and the $C^\beta H^\beta$ bond distance are not much different from those at the corresponding initial geometries. On the other hand, the skeletal bond distances change greatly from those at the corresponding initial geometries. Consequently, the benzene ring changes from an aromatic to a quinoid structure. In addition, the ethynyl part comes to take an incomplete allenoid skeleton structure. In Figure 7, we show geometrical changes along the reaction coordinate starting from the largest initial bent geometry of S_0B21. They are similar to those of S_0 geometry in Figure 2b,c, except for bend angle β at the early stage. Therefore, we can conclude that each inflection point is the ending point of PR1 as well as the starting point of PR2. At each inflection point, in other words, hybridization of the C^β atom switches from sp into sp^2, although the position is strongly dependent on the initial bend angles. These discussions foster the conclusion that electronically excited PA in S_2 around the S_0 geometry takes a similar path to reach the most stable S_2-bent geometry. That is, the skeletal π-conjugated system is first destroyed to form an incomplete allenoid structure, and then an out-of-plane bending of the H^β atom takes place to form a complete allenoid structure, irrespective of the initial bend angle. However, we can also find that the initial $C^\beta H^\beta$ OP

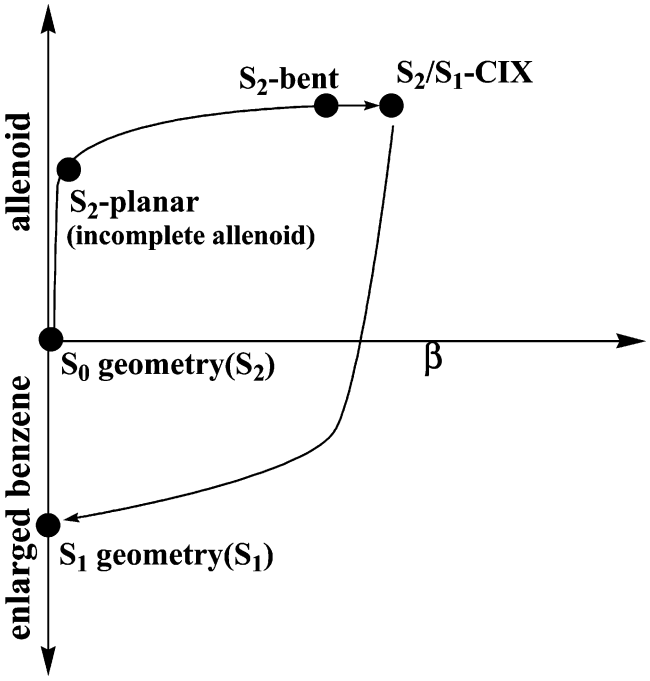

Figure 4. Schematic representation of the S_2-S_1 internal conversion of PA. The meanings of allenoid and enlarged benzene on the ordinate are described in Appendix 1.

bending motion in S_0 clearly affects the dynamics. Figure 5 shows that a larger initial bend angle β indicates a shorter distance to an inflection point (shown digitally in Table 2) as well as a stable region of the S_2-bent geometry. This fact implies that a more violent initial $C^{\beta}H^{\beta}$ OP bending motion will cause PA to reach the S_2-bent geometry more quickly. Later, we will comment further on the initial bending motion.

3.4. Dipole Moments along the Reaction Coordinate. The dipole moment as a function of reaction coordinate provides new insight into the substituent effect of the ethynyl group on the IC process. Table 3 lists the *y* and *z* components of the dipole moments (see Figure 1 for the directions of the *x*, *y*, and *z* axes). The *x* component is essentially zero in processes PR1−PR4 because PA retains almost complete C_s symmetry (the *yz* plane is the symmetry plane). Therefore, our concern is only the *y* and *z* components (μ_y and μ_z) as a function of the reaction coordinate. Actually, μ_y is a good measure for the degree to which the H^{β} atom deviates from the plane of the other part. In PR1, μ_y is fundamentally 0 D because PA takes a planar structure. In PR2, in turn, the μ_y component becomes large in concert with the decrease of the bend angle β. In PR3, μ_y remains almost unchanged because the bend angle is little changed. In PR4, μ_y quickly converges to 0 D because the ethynyl part recovers its linear shape in S_1.

The *z* component μ_z exhibits an extremely interesting behavior along the reaction coordinate. The μ_z component in S_0 at the S_0 geometry takes a small negative value (−0.555 D), meaning that the electron is transferred slightly from the benzene ring into the ethynyl part. Such behavior is consistent with a well-known finding that the ethynyl group is electron-withdrawing, but the electron-withdrawing capability is much weaker than that of an isoelectronic molecule of benzonitrile (−4.831 D); they are compared in Table 3. Upon electronic excitation of S_2 at the S_0 geometry (i.e., $s_A = 0.0$), however, μ_z suddenly takes a large positive value (2.796 D). This change indicates that the ethynyl part changes from an electron-withdrawing to an electron-donating group through electronic excitation into S_2, whereas it does not change through electronic excitation into S_1. Table 3 shows the Mulliken charge in each fragment. Apparently, a large positive value of μ_z in S_2 is ascribed to the electron transfer from the ethynyl into the phenyl group. This electron transfer serves to destroy the aromatic benzene ring and to form a quinoid structure. At the S_2-planar geometry, μ_z takes a much smaller value, but it is still positive, which is ascribed to a skeletal relaxation on the S_2 surface. In PR2, μ_z changes from positive to negative values in coincidence with the decrease of bend angle β and the further elongation of the $C^{\alpha}C^{\beta}$ bond. These geometrical changes serve to push electrons back into the terminal $C^{\beta}H^{\beta}$ part. In PR4, after the transition at S_2/S_1-CIX (i.e., $s_{BC} = 0.0$), μ_z converges quickly to the value at the S_1 geometry in coincidence with the formation of the S_1 geometry.

The dipole moment, which is dependent on the reaction coordinate, is closely related to the successive geometrical changes described above. That is, the sudden change of the electron-withdrawing group into an electron-donating group upon electronic excitation into S_2 is a trigger for an effective and fast S_2-S_1 IC process of PA. Additionally, we comment on the effect of the initial $C^{\beta}H^{\beta}$ OP bending mode on the dipole

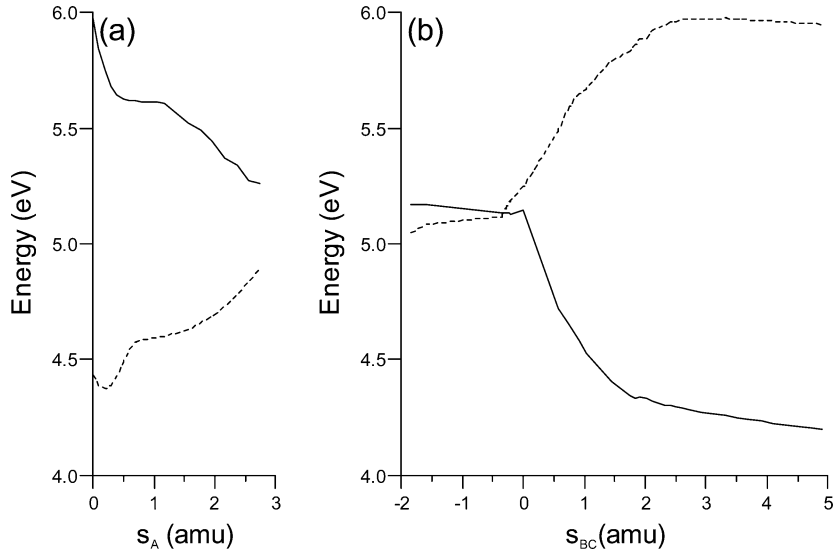

Figure 5. Potential energy profiles (solid line) along the reaction coordinate using MRMP2 with the (10,10)CASSCF wave function. The dotted line represents the potential energy of the counter state. (a) Path A. (b) Paths B and C.

TABLE 2: Summary of the Features at Inflection Points in S_2

initial geometry inflection point[a]	S_0 geometry 0.895	S_0B05 0.698	S_0B10 0.649	S_0B15 0.599	S_0B21 0.500
			Bond Distances (Å)		
$R(C^{\alpha}-C^{\beta})$	1.290 (1.215)[b]	1.291[c]	1.292	1.291	1.285
$R(C^1-C^{\alpha})$	1.360 (1.448)	1.360	1.361	1.364	1.373
$R(C^1-C^2)$	1.469 (1.405)	1.458	1.453	1.449	1.441
$R(C^2-C^3)$	1.367 (1.398)	1.366	1.367	1.369	1.373
$R(C^3-C^4)$	1.462 (1.401)	1.445	1.439	1.434	1.426
$R(C^4-C^5)$	1.462 (1.401)	1.445	1.439	1.434	1.426
$R(C^5-C^6)$	1.367 (1.398)	1.366	1.367	1.369	1.373
$R(C^{\beta}-H^{\beta})$	1.057 (1.058)	1.058	1.058	1.058	1.057
			Bond Angles (deg)		
$\beta(-C^{\alpha}C^{\beta}H^{\beta})$	180.0 (180.0)	174.7 (177.3)[d]	171.0 (174.6)	168.0(171.9)	165.5(168.5)
			Dipole Moments (D)		
μ_z	0.689 (2.796)	0.780 (2.787)	0.762 (2.756)	0.763 (2.708)	0.883 (2.620)
μ_y	−0.001 (0.0)	0.147 (0.071)	0.250 (0.141)	0.328 (0.211)	0.394 (0.296)

[a] s_A in amu. [b] Values in the parentheses are those at S_0 geometry. [c] Values of the bond distances at the initial bent geometries, which are not shown, are the same as those at S_0 geometry. [d] Values in parentheses are those at the initial bent geometries.

TABLE 3: Dipole Moment Components and Mulliken Charges at Important Conformations of PA and Related Molecules[a]

reaction coordinate (amu)	state	dipole moment (D)		Mulliken charge		
		μ_z	μ_y	$C^{\beta}H^{\beta}$	C^{α}	phenyl
			Phenylacetylene			
$s_A = 0.0$ (S_0 geometry)	S_0	−0.555	0.0	−0.185	0.060	0.125
	S_1	−0.546	0.0	−0.188	0.066	0.122
	S_2	2.796	0.0	−0.127	0.166	−0.039
$s_A = 0.0$ (S_0B21)	S_2	2.620	−0.296	−0.125	0.157	−0.032
$s_A = 0.895$ (S_2-planar)[b]	S_2	0.689	0.0	−0.161	0.093	0.068
$s_A = 1.566$	S_2	0.247	−0.430	−0.147	0.054	0.093
$s_A = 1.966$	S_2	−0.253	−0.625	−0.129	0.010	0.119
$s_A = 2{,}936$ (S_2-bent)[b]	S_2	−1.158	−0.793	−0.115	−0.025	0.140
$s_{BC} = 0.0$ (S_2/S_1-CIX)	S_1	−1.519	−0.795	−0.114	−0.032	0.146
$s_{BC} = 1.033$	S_1	−0.966	−0.405	−0.160	0.029	0.131
S_1 geometry	S_1	−0.503	0.0	−0.186	0.074	0.112
			Benzonitrile[b]			
S_0 geometry	S_0	−4.831	0.0	−0.159	−0.087	0.246

[a] Strictly speaking, $s_A = 0.895$ is not the S_2-planar geometry because the configuration of the S_2-planar geometry in Table 1 is obtained under the constraint of C_{2v} symmetry, whereas the geometry at $s_A = 0.895$ is not. However, the two geometries are substantially identical; we call $s_A = 0.895$ the S_2-planar geometry, for convenience. Using similar reasoning, the geometry at $s_A = 2.936$ is called the S_2-bent geometry. [b] Geometry was optimized at the restricted Hartree−Fock level with a similar basis set (i.e., DZ plus polarization for C and N atoms, DZ for H atoms).

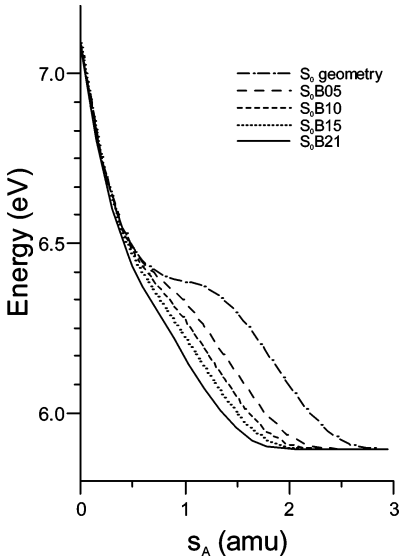

Figure 6. Potential energy profiles along the reaction coordinate from the initial bent geometries and S_0 geometry.

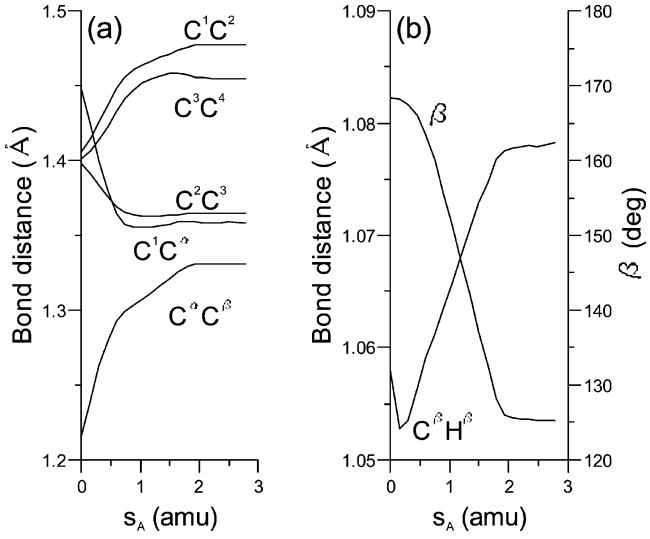

Figure 7. Characteristic geometrical parameters along the reaction coordinate from S_0B21: (a) changes of bond distances of the PA skeleton, (b) changes of the $C^{\beta}H^{\beta}$ bond distance and $-C^{\alpha}C^{\beta}H^{\beta}$ bending angle β.

moment. As Table 2 shows, the μ_x and μ_z components at each inflection point do not differ greatly from their corresponding initial values. This lack of change reflects the fact that electronically excited PA in S_2 around the S_0 geometry follows a route in PR1 similar to that indicated above.

TABLE 4: Vibrational Frequencies (cm^{-1}) of the ν_5 Band

reaction coordinate	state	frequency[a]
$s_A = 0.0$ (S_0 geometry)	S_0	2126 (2120[b])
0.0	S_2	2035
0.100	S_2	1991
0.200	S_2	1942
0.895	S_2	1909
$s_{BC} = 0.0$(S_2/S_1-CIX)	S_1	1806
0.296	S_1	1805
0.569	S_1	1861
0.752	S_1	1928
0.908	S_1	1963
1.033	S_1	1983
1.222	S_1	2004
1.373	S_1	2017
1.500	S_1	2025
S_1 geometry	S_1	2055 (2065[c])

[a] Force constants are commonly scaled down by 0.90, but those related to C−H stretches are scaled down by 0.82. [b] Experimental result taken from ref 16. [c] Experimental result taken from ref 12.

3.5. Vibrational Analysis along the Reaction Coordinate. The vibrational analysis along the reaction coordinate can be closely related to the temporal behavior in the IC process, which can be verified through a time-resolved transient spectroscopic experiment. Table 4 shows the vibrational frequency of the ν_5 band of the $C^{\alpha}C^{\beta}$ stretch as a function of reaction coordinate. To the extent that PA stays in S_2, the characteristic $C^{\alpha}C^{\beta}$ stretch is expected to be observed in the region of 2000−1800 cm^{-1}, which is a typical region of allenoid stretch frequencies. Actually, by means of a direct absorption spectroscopic experiment that reflects the early stage after electronic excitation into S_2, the characteristic allenoid stretch is observed in 1846 ± 15 cm^{-1}.[13] On the other hand, once PA relaxes into S_1, the $C^{\alpha}C^{\beta}$ stretch in the allenoid region disappears quickly and emerges in the C≡C triple bond region. These discussions imply that a characteristic transient absorption band is expected to be observed in the allenoid region only during a short period in S_2 (54 fs at most, by experimental estimation[3]).

Furthermore, we can point out the following aspects of the behavior of PA in S_2 in relation to a spectroscopic experiment. One is that the $C^{\alpha}C^{\beta}$ stretch frequency in S_2 is strongly dependent on the reaction coordinate even in the allenoid region: the vibrational frequency decreases quickly from 2000 to 1800 cm^{-1}. The other is that the initial $C^{\beta}H^{\beta}$ OP bending motion affects the time to reach the stable S_2-bent geometry after electronic excitation into S_2. That is, a higher temperature yields more species with vibrationally excited $C^{\beta}H^{\beta}$ OP motion around the S_0 geometry. Consequently, the lifetime in S_2 after electronic excitation is expected to be shorter. However, these conjectures might be difficult to verify experimentally for the moment because the S_2-S_1 IC process is too fast.

4. Concluding Remarks

In this article, we reported the reaction coordinate of the S_2-S_1 IC of PA. Analyses of the reaction coordinate show that several internal coordinates couple strongly with each other in the S_2-S_1 IC process. Upon electronic excitation into S_2, the aromatic benzene ring becomes a quinoid structure, and the ethynyl part changes into an incomplete allenoid skeleton. Then, PA takes a complete allenoid structure of the ethynyl part to reach S_2/S_1-CIX where the radiationless relaxation takes place. Once PA relaxes into S_1 at S_2/S_1-CIX, it changes quickly into the most stable geometry in S_1, which is characterized by an enlarged benzene ring. The strong mode couplings among the internal coordinates on the multidimensional potential energy surfaces in S_1 and S_2 bring about an effective internal vibrational redistribution. Thereby, the S_2-S_1 IC process is very fast: on the order of several tens of femtoseconds. The dipole moment component that is parallel to the long axis is strongly dependent on the electronic state and conformation. In S_0 and S_1, it is confirmed that the ethynyl group is a weak electron-withdrawing group. Upon electronic excitation of S_2, on the other hand, the ethynyl group changes to become an electron-donating group, which induces PA to form a quinoid structure at the early stage. Results of vibrational analysis along the reaction coordinate show that the characteristic key band of the allenoid stretch is strongly dependent on the conformation and the electronic state in the S_2-S_1 IC process.

Acknowledgment. We are grateful to Dr. Stolow (National Research Council of Canada) who informed us of recent experimental work related to π-conjugated systems. Numerical calculations were performed partly at the Computer Center of Institute for Molecular Science. This work was supported financially by a Grant-in-Aid for Scientific Research from the Japan Society for the Promotion of Science.

Supporting Information Available: All Cartesian coordinates at the important conformations mentioned in section 3.1 are available via the Internet at http://pubs.acs.org.

Appendix 1

Figure 4 presents three coordinates to clarify the IC process. The "allenoid" coordinate in the upper ordinate represents the degree to which the ethynyl part ($-C^{\alpha}\equiv C^{\beta}H^{\beta}$) takes an allenoid structure ($=C^{\alpha}=C^{\beta}H^{\beta}$). As mentioned above, the formation of the allenoid structure is related closely to that of the quinoid structure in the benzene ring. Therefore, the allenoid coordinate also involves the degree to which PA loses its aromaticity in the benzene ring. The "enlarged benzene" in the lower ordinate represents the degree to which the benzene ring expands with the hexagon. The abscissa represents the $-C^{\alpha}C^{\beta}H^{\beta}$ bend angle β.

Appendix 2

The calculated ν_{29} band of 597 cm^{-1} (613 cm^{-1} by experiment[16]) is assigned to the $C^{\beta}H^{\beta}$ OP mode because the L-matrix component (0.970) related to the $C^{\beta}H^{\beta}$ OP mode is almost unity. For that reason, we estimated the largest OP deviation from the S_0 geometry by the calculated ν_{29} vibration. The results showed that only the y component of the H^{β} atom takes a large value (0.2113 Å); the others are very small (less than 0.0220 Å). Therefore, we put the H^{β} atom at $y = 0.21$ Å, keeping the $C^{\beta}H^{\beta}$ bond distance at that of the S_0 geometry.

References and Notes

(1) Stock, G.; Domcke, W. *Adv. Chem. Phys.* **1997**, *100*, 1−169.

(2) Stolow, A. *Annu. Rev. Phys. Chem.* **2003**, *54*, 89−119.

(3) Polivka, T.; Zigmantas, D.; Frank, H. A.; Bautista, J. A.; Herek, J. L.; Koyama, Y.; Fujii, R.; Sundstrom, V. *J. Phys. Chem. B* **2001**, *105*, 1072−1080.

(4) Lee, S.-H.; Tang, K.-C.; Chen, I.-C.; Underwood, J. G.; Stolow, A.; Schmitt, M.; Shaffer, J. P.; Schultz, T.; Zgierski, M. Z. *J. Phys. Chem. A* **2002**, *106*, 8979−8991.

(5) Fuss, W.; Pushpa, K. K.; Rettig, W.; Schmid, W. E.; Trushin, S. A. *Photochem. Photobiol. Sci.* **2002**, *1*, 255−262.

(6) McCamant, D. W.; Kukura, P.; Mathies, R. A. *J. Phys. Chem. A* **2003**, *107*, 8208−8214.

(7) Shah, B. K.; Rodgers, M. A. J.; Neckers, D. C. *J. Phys. Chem. A* **2004**, *108*, 6087−6089.

(8) Domcke, W.; Yarkony, D. R.; Köppel, H. *Conical Intersections, Electronic Structure, Dynamics & Spectroscopy*; Advanced Series of Physical Chemistry; World Scientific Publishing Co. Pty. Ltd.: Singapore, 2004; Vol. 15.

(9) Amatatsu, Y.; Hasebe, Y. *J. Phys. Chem. A* **2003**, *107*, 11169−11173.

(10) Amatatsu, Y. *Chem. Phys. Lett.* **1999**, *314*, 364−368; *Chem. Phys. Lett.* **2001**, *344*, 200−206; *J. Comput. Chem.* **2002**, *23*, 950−956, *Chem. Phys. Lett.* **2003**, *369*, 673−679; *THEOCHEM* **2003**, *624*, 159−167; *J. Phys. Chem. A* **2005**, *109*, 7225−7235.

(11) Amatatsu, Y.; Hosokawa, M. *J. Phys. Chem. A* **2004**, *108*, 10238−10244.

(12) King, G. W.; So, S. P. *J. Mol. Spectrosc.* **1971**, *37*, 543−570.

(13) Ribblett, J. W.; Borst, D. R.; Pratt, D. W. *J. Chem. Phys.* **1999**, *111*, 8454−8461.

(14) Leopold, D. G.; Hemley, R. J.; Vaida, V.; Roebber, J. L. *J. Chem. Phys.* **1981**, *75*, 4758−4769.

(15) Schmidt, M. W.; Baldridge, K. K.; Boatz, J. A.; Elbert, S. T.; Gordon, M. S.; Jensen, J. H.; Koseki, S.; Matsunaga, N.; Nguyen, K. A.; Su, S. J.; Windus, T. L.; Dupuis, M.; Montgomery, J. A., Jr. *J. Comput. Chem.* **1993**, *14*, 1347−1363.

(16) King, G. W.; So, S. P. *J. Mol. Spectrosc.* **1970**, *36*, 468−487.